02,03,14

The effect of a thin protective ScN coating on the superconducting and structural properties of ultrathin NbN films

© N.V. Porokhov[1,2], A.A. Anikanov[1], A.A. Shibalova[1], M.V. Shibalov[1], G.D. Diudbin[1], A.M. Mumlyakov[1], I.V. Trofimov[1], N.A. Vovk[1], M.A. Tarkhov[1,2]

[1] Institute of Nanotechnology of Microelectronics, Russian Academy of Sciences, Moscow, Russia
[2] National Research University „Moscow Power Engineering Institute“, Moscow, Russia

E-mail: nporokhov@gmail.com

Received July 8, 2024
Revised July 8, 2024
Accepted July 11, 2024

The influence of a thin scandium nitride (ScN) protective layer on the superconducting properties of niobium nitride (NbN) thin films deposited by reactive magnetron sputtering was investigated. A comprehensive analysis of the morphological, microstructural, and electrophysical properties of the thin films subjected to high-temperature annealing in an oxygen atmosphere is presented. The dependence of the critical transition temperature of the NbN thin film on the annealing temperature in an oxygen environment, both with and without the ScN coating, was established. X-ray reflectometry studies revealed that the ScN film serves as a protective layer even at annealing temperatures around 450°C, without affecting the density and thickness of the NbN layer. It was demonstrated that the NbN thin film coated with an ScN layer is more resistant to aggressive environments than the uncoated NbN film.

Keywords: superconductivity, protective coatings, niobium nitride, scandium nitride, thin films.

DOI: 10.61011/PSS.2024.09.59210.182

1. Introduction

Niobium nitride is widely used to produce superconductor nanoelectronic devices of various functional purpose, e.g. single-photon detectors SNSPD [1], HEB bolometers and mixers of THz range on hot electrons [2], microwave kinetic inductance detectors (MKIDs) [3] etc. Thin films NbN are produced by various methods: reactive magnetron sputtering of niobium target in gas mixture of Ar and N_2 [4], pulse-laser deposition (PLD) [5], high temperature chemical vapor deposition (HTCVD) and atomic layer deposition (ALD) [6]. NbN films also demonstrate high compatibility with CMOS technology [7]. Due to their volatility in fluorine-containing compounds, they can be easily treated in industrial systems of plasma-enhanced chemical etching [8]. Many stages of the technological process, associated with manufacturing of superconductor electronics, can be accompanied by high temperature and chemically aggressive atmosphere, this increases probability of degradation of the functional layer of components [9,10]. Due to this the studies of materials of ultrathin protective layers not affecting properties of functional thin films are actual. Scandium nitride has high mobility of electrons, high hardness, high melt point and corrosion resistance [11,12]. All this makes scandium nitride a promising material for manufacturing of wear-resistant and protective coatings on surfaces of various materials [13].

In present paper we studied the effect of ultrathin protective layer ScN 10 nm thick on the electrophysical properties of thin films NbN, obtained by reactive magnetron sputtering. The comprehensive analysis of morphological, microstructural and electrophysical characteristics of thin films after process of high-temperature annealing in oxygen environment was performed. The morphology of the obtained films was studied by the atomic force microscopy (AFM). Structural studies of the obtained films were performed by methods of transmission and high-resolution transmission electron microscopy (TEM and HRTEM, respectively). Main method of thickness and density measurement of functional films before and after annealing is method of X-ray reflectometry (XRR). The electrophysical properties of films were determined at room temperature and at cryogenic temperatures.

2. Experiment

Samples of two compositions were analyzed: NbN|ScN — structure Si (*n*-type) $|SiO_2|$NbN|ScN; NbN — structure Si (*n*-type) $|SiO_2|$NbN. Silicon substrate Si (*n*-type) with amorphous thermal oxide 500 nm thick was basis of both compositions. After the magnetron sputtering application NbN thin layer 13 nm thick was deposited, then *in situ* ScN thin layer 10 nm thick was deposited (see Figure 1).

The thin layers of nitrides were deposited by method of reactive magnetron sputtering from targets of niobium and

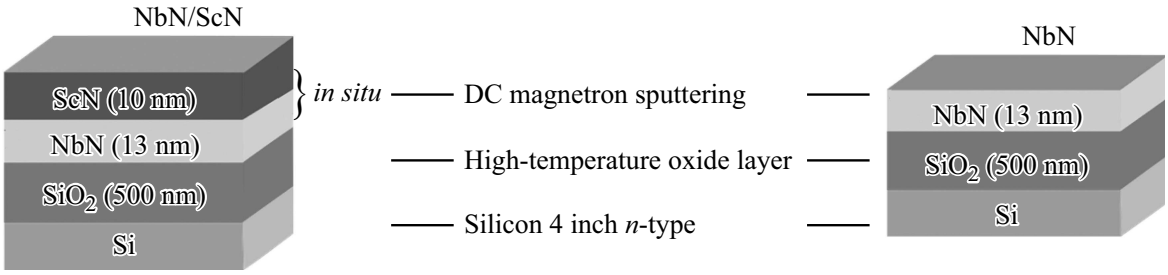

Figure 1. Schematic image of samples under study.

scandium with high purity (99.999%). The process was performed in atmosphere of inert gas mixture comprising argon and nitrogen, at room temperature, with ratio argon : nitrogen 4 : 1 respectively. Direct current power of magnetron was maintained at level of 5 W/cm^2. Under these conditions the layer deposition rate was 11 nm/min.

Then samples were subjected to degradation by oxygen annealing at different temperatures. The annealing procedure was performed in a diffusion pipe, the sample was heated to set annealing temperature in nitrogen atmosphere, then temperature stabilization was performed for 10 min, and after that annealing in oxygen atmosphere was performed for 30 min. Heating rate was 5°C/min, and cooling rate — 2°C/min. As during annealing two factors present, which can affect the fil properties (temperature and composition of environment), then additional series of annealing of compositions NbN|ScN in nitrogen in temperature range 350−550°C was performed to exclude occurrence of degradation exactly due to temperature.

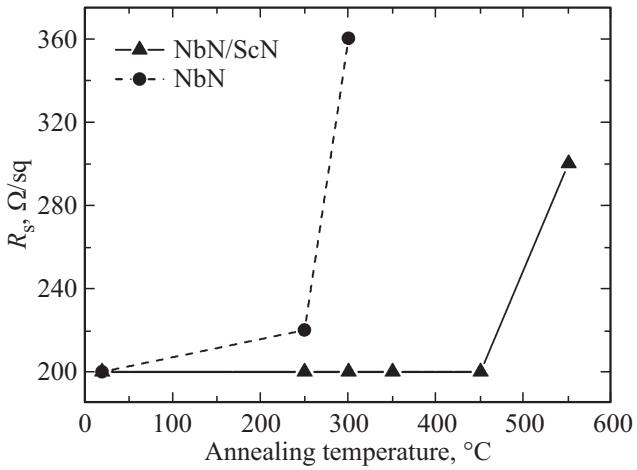

Figure 2. Surface resistance of film R_s vs. temperature of oxygen annealing. Solid line — values for composition NbN, dashed line — for composition NbN|ScN.

3. Results

Input parameter of film conductivity is value of its surface resistance R_s, which ensures evaluation of degradation rate of conductive layer of sample at different annealing temperatures. Value of surface resistance of films was determined by four-probe method [14]. Values of surface resistance vs.annealing temperature for samples of composition NbN|ScN are presented in Figure 2 (solid line). From graph we see that below temperature 450°C values R_s do not change, but at 550°C resistance increases, and at temperatures 650°C and above the conductive layer transforms into dielectric. Figure 2 also provides dependence for composition NbN (dashed line). It is obvious, that degradation of the conductive layer occurs at lower annealing temperatures as compared to composition NbN|ScN.

Cryogenic measurements were performed in Gifford-McMahon closed cycle cryostat, where dependence of sample resistance on temperature $R(T)$ were taken. To determine value of the critical transition temperature T_c and transition width ΔT_c the graph of dependence $R(T)$ was transformed into the graph of dependence $\frac{dR}{dT}(T)$. Maximum value of this function corresponds to T_c, and width at half maximum of graph corresponds to width of sample transition into superconducting state. Figure 3 presents experimental dependences of normalized resistance on temperature for samples of compositions NbN (a) and NbN|ScN (b) at different temperature modes of annealing. Ratio of width of transition into superconducting state between initial samples and samples subjected to practically full oxidation for both compositions was 1.5 times. Note that width of transition into superconducting state of composition NbN|ScN practically did not change until annealing temperature 450°C (Figure 3, b).

As expected, for composition NbN the critical temperature T_c decreases with annealing temperature increasing (Figure 4, dashed line), and already at temperatures above 350°C composition NbN transforms into dielectric. For composition NbN|ScN change in critical temperature T_c remains insignificant at annealing temperatures below 450°C. But upon annealing temperature increasing above 450°C significant change in critical temperature of transition occurs (Figure 4, solid line). No cryogenic measurements were

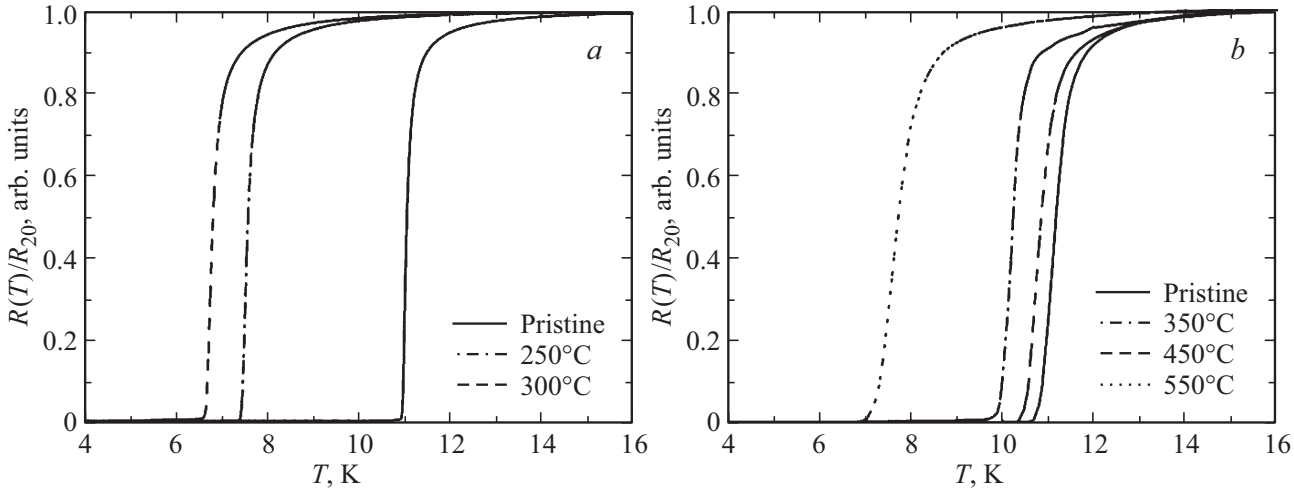

Figure 3. Normalized resistance vs. temperature: *a*) for composition NbN; *b*) for composition NbN|ScN after oxygen annealing.

performed for samples that during annealing transformed into dielectrics.

The critical current was measured in accordance with double-point diagram of measurements using current source Keithley 6221A with high accuracy and minimum noise level. The dependence of critical current density on temperature was analyzed based on current-voltage curves (CVCs). CVCs were measured in mode of voltage stabilization in temperature range from 2.5 K and to temperature of transition into resistive state. Value of critical current I_c was determined as current corresponding to complete structure transformation from superconducting state into resistive state. Dependences of critical current density temperature were plotted for composition NbN|ScN at different annealing temperatures. Current critical density $J_c(T)$ was calculated as $I_c(T)/(w \cdot d)$, where w — width of superconducting strip, and $d = 13$ nm (thickness of film NbN). Set of temperature dependences J_c is shown in Figure 5, *a*, solid lines demonstrate the theoretical dependence of de-pairing critical current, described by Ginzburg-Landau theory [15]. Figure 5, *b* presents critical current density at liquid helium temperature (4.2 K) vs. annealing temperature, in insert SEM image of bridge topology with smooth input is presented. Similarly to critical temperature the graph of critical current density vs. annealing temperature demonstrates similar behavior. Significant changes in value of the current critical density occur at annealing temperature above 450°C.

The surface morphology was studies before and after oxygen annealing. The atomic-force microscopy (AFM) was used to determine the surface roughness parameter. The surface roughness of films was performed on area $1\,\mu m^2$ in semicontact mode. After results processing the roughness parameters R_q were obtained for set regions, where R_q — means square deviation of surface height from weighted average value. Figure 6 presents graphs of

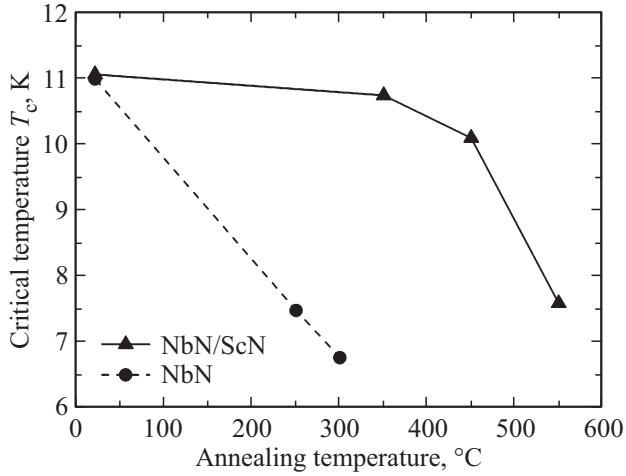

Figure 4. Critical temperature of transition of samples of compositions NbN|ScN and NbN vs. annealing temperature of samples in oxygen atmosphere.

dependences of R_q on annealing temperature of samples of two compositions.

Graph shows that surface morphology of film ScN of composition NbN|ScN drastically does not change until 550°C, and only at temperature above 550°C the surface morphology changes, it appears in form of abrupt jump of value of roughness parameter at 650°C. Samples of composition NbN demonstrate morphology changes at significantly lower temperatures, namely, the roughness parameter changes at temperature above 250°C.

Main method of thickness and density measurement of functional films before and after annealing is method of X-ray reflectometry (XRR). Figure 7 presents experimental results of X-ray reflectometry of samples of composition NbN (*a*) and NbN|ScN (*b*), initial sample, ans sample after oxygen annealing for 30 min in temperature range of 250 to 750°C.

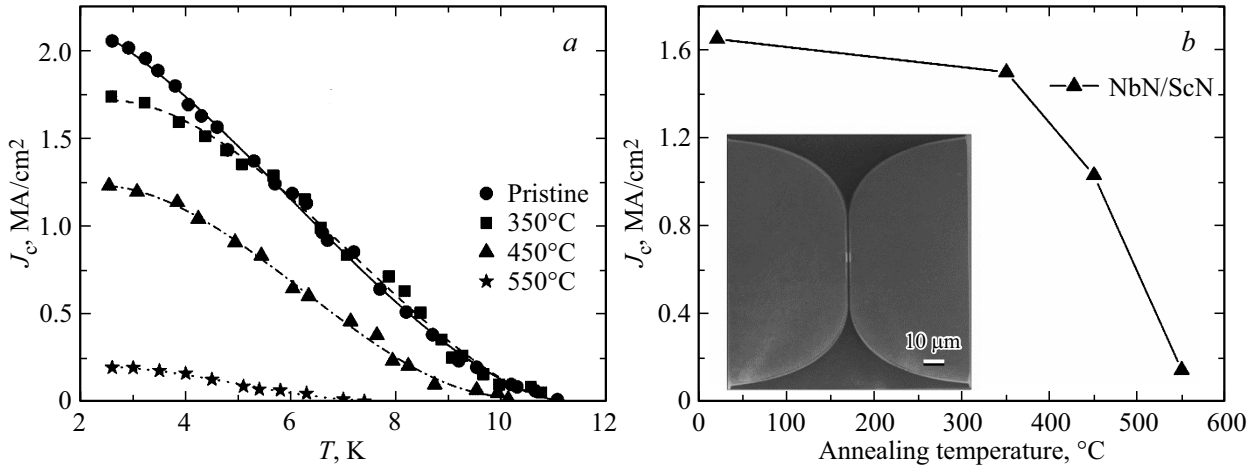

Figure 5. *a*) For compositions NbN|ScN at different annealing temperatures critical current densities vs. temperature; *b*) critical current density at temperature 4.2 K vs. annealing temperature of samples of composition NbN|ScN.

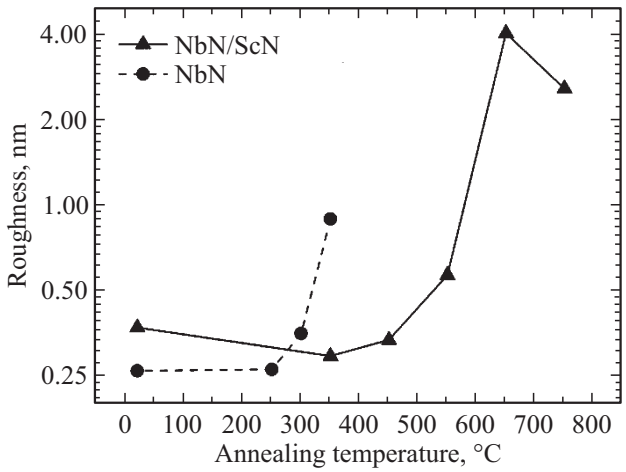

Figure 6. Graph of roughness parameter vs. annealing temperature of samples for two compositions.

Curves analysis of X-ray reflectometry for composition NbN shows that at annealing temperature equal to 350°C, there is complete oxidation of the functional layer NbN with transition into less dense material Nb_xO_y. As a result of studies of composition NbN it was identified that functional film degrades at annealing temperatures 350°C in oxygen atmosphere. From sturdy results of X-ray reflectometry of composition NbN|ScN it follows that ultrathin film ScN plays the role of protective layer below temperatures 450°C in oxygen medium, at that not demonstrating effect on density and thickness of the functional layer NbN, this is confirmed by study by method of transmission electron microscopy (TEM).

Figure 8 presents TEM results for initial sample and after annealing in oxygen at 350, 450, 550 and 650°C. Layers are arranged such: bottom layer — silicon oxide, dark layer with high density — NbN_x ~ 12.5 nm thick, further light layer with low density — ScN_x ~ 7.5 nm thick, further surface layer below 3 nm and top layer — protective layer of platinum. Each TEM photo in right side contains graph of density dependence on depth from data of X-ray reflectometry. Data Comparison of TEM and XRR shows high degree of data convergence. For sample after annealing at 550°C as per results of both TEM, and XRR the protective layer ScN begins to demonstrate changes, it is oxidated. At that at interface ScN|NbN a thin layer ~ 1.5 nm thick is formed, and total thickness of NbN decreasing by ~ 1 nm is visible. Thus we can suppose that at 550°C layer NbNx is partially oxidated. At same time the sample subjected to annealing at 650°C, demonstrates strong changes occurred both in layer ScN, and in layer NbN. Structure of both films is heterogeneous: through thickness of each film a large number of cavities, regions with decreased density and different crystalline structure is observed. From Figure 8, *e* we see also that roughness of interface ScN|NbN significantly increased, separation to layers still occurs and is visually observed by contrast of layers NbN and ScN in TEM-images. As per data of TEM and XRR, after annealing at 650°C thickness of layers ScN and NbN significantly increased, and by HRTEM results it is ~ 11 and ~ 31 nm respectively unlike ~ 12.5 and ~ 7.5 nm in initial sample and in sample after annealing up to 550°C.

The results of the studies show that ScN thin film 10 nm thick has high thermal and chemical stability, which makes it a promising thin-film material for use in high-temperature conditions and aggressive chemical environments. These conclusions are based on the experimental data shown above. But the issue, what exact factors affect the sample properties during annealing, stays unsolved. For detail understanding of this issue we performed additional series of experiments including annealing of composition NbN|ScN in nitrogen medium at same temperature mode, with oxygen exclusion.

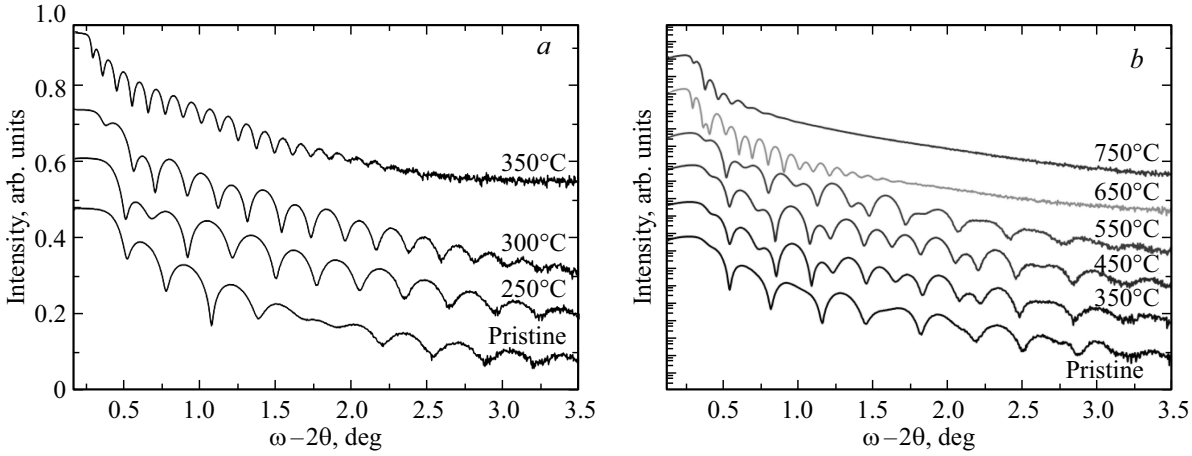

Figure 7. Curves of X-ray reflectometry: *a*) composition NbN; *b*) composition NbN|ScN, at different annealing temperatures.

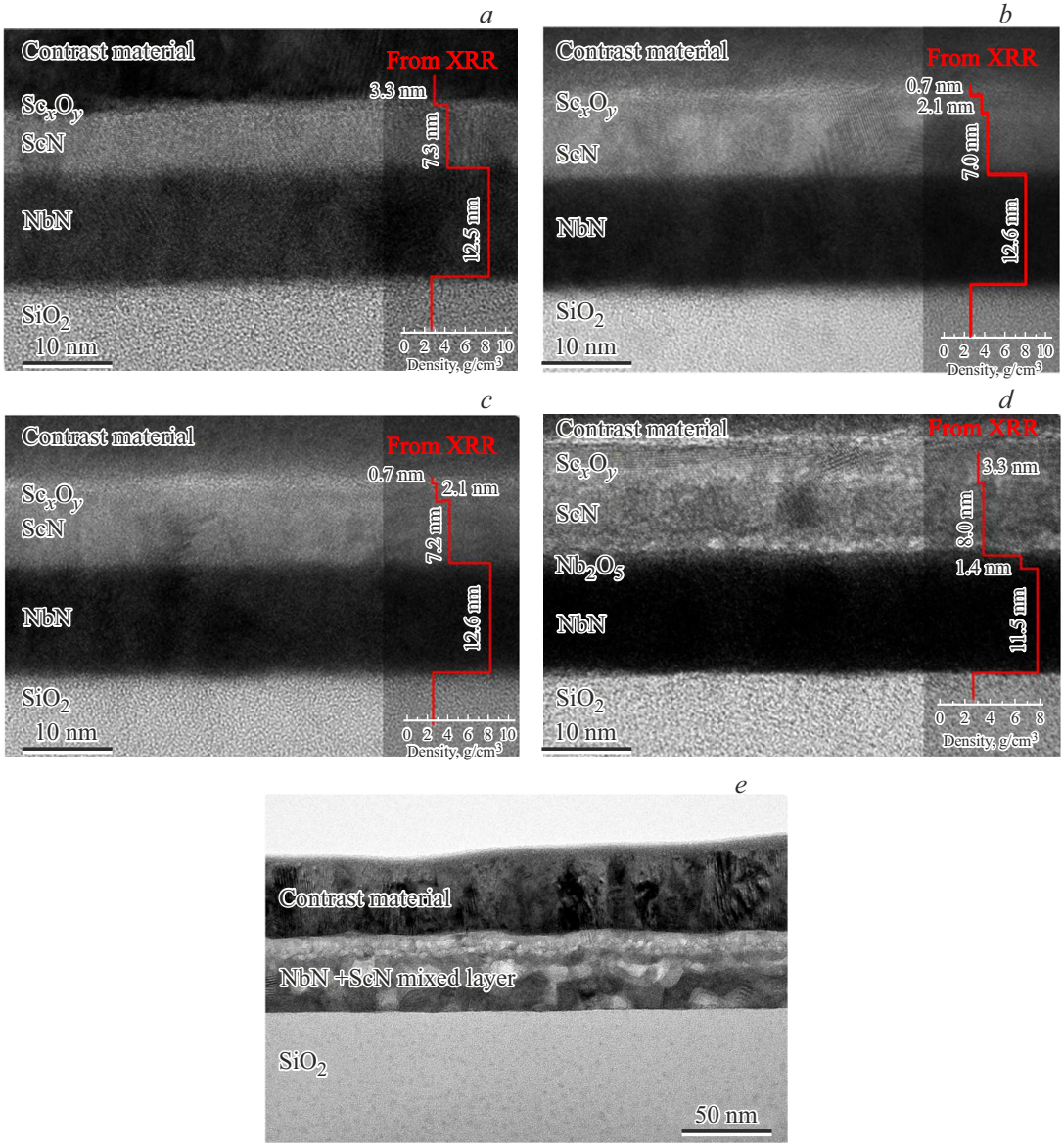

Figure 8. TEM-images of cross-section: *a*) initial composition NbN|ScN and samples after oxygen annealing at temperatures: *b*) 350°C, *c*) 450°C, *d*) 550°C, *e*) 650°C.

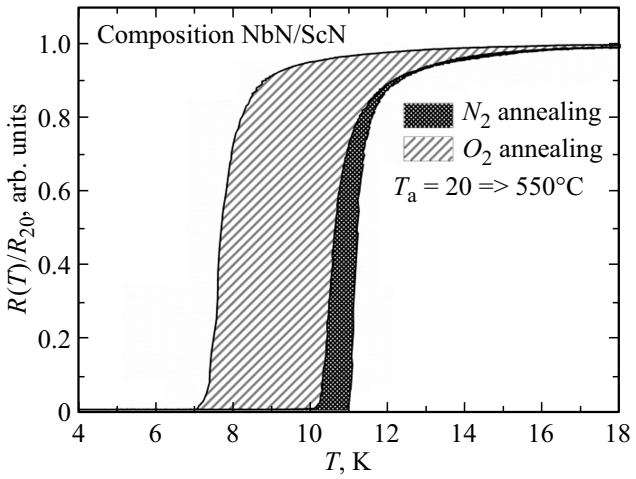

Figure 9. Comparative diagram of dependences of normalized resistance on temperature of samples of composition NbN|ScN after heat treatment in nitrogen (fine shading) and oxygen (coarse shading) mediums.

In presented diagram in Figure 9 the comparative dependences are shown of normalized resistance on temperature of samples of composition NbN|ScN after heat treatment in nitrogen and oxygen mediums in temperature range of 20 to 550°C. Graph analysis provides statement that change in superconducting properties of samples during high-temperature annealing if directly associated with action of oxygen from environment.

4. Conclusion

During study of the protective effect of ScN thin film, it is found that its thickness of 10 nm provides high stability both thermally and chemically. Studies of X-ray reflectometry show that ScN film executes function of the protective layer even at annealing temperature near 450°C, without effect on density and thickness of NbN layer. It is demonstrated that NbN thin film coated with ScN film is more resistive to aggressive medium than film without ScN coating. All this indicates the perspectivity of material for use in conditions of elevated temperatures and aggressive chemical mediums.

Acknowledgments

The authors express their gratitude to P.A. Neklyudova and E.M. Eganova for assistance in preparing samples for TEM, as well as to Yu.P. Korneeva for preparing samples and performing cryogenic measurements.

Funding

This study was supported by project No. 122040800153-0 of the Ministry of Science and Higher Education of the Russian Federation. The study was carried out using equipment from the LSRF ECHIT of Institute of Nanotechnology Microelectronics of the Russian Academy of Sciences.

Conflict of interest

The authors declare that they have no conflict of interest.

References

[1] C.M. Natarajan, M.G. Tanner, R.H. Hadfield. Supercond. Sci. Technol. **25**, *6*, 063001 (2012). https://doi.org/10.1088/0953-2048/25/6/063001, arXiv:1204.5560
[2] T.M. Klapwijk, A.V. Semenov. IEEE Trans. Terahertz Sci. Technol. **7**, *6*, 627 (2017). https://doi.org/10.1109/TTHZ.2017.2758267
[3] S. Ariyoshi, K. Nakajima, A. Saito, T. Taino, H. Tanoue, K. Koga, N. Furukawa, H. Yamada, S. Ohshima, C. Otani, J. Bae. Appl. Phys. Express **6**, *6*, 064103 (2013). https://doi.org/10.7567/APEX.6.064103
[4] J.J. Olaya, L. Huerta, S.E. Rodil, R. Escamilla. Thin Solid Films **516**, *23*, 8768 (2008). https://doi.org/10.1016/j.tsf.2008.06.065
[5] S. Volkov, M. Gregor, T. Roch, L. Satrapinskyy, B. Grančič, T. Fiantok, A. Plecenik. J. Electr. Eng. **70**, *7*, 89 (2019). https://doi.org/10.2478/jee-2019-0047
[6] M.V. Shibalov, A.M. Mumlyakov, I.V. Trofimov, E.R. Timofeeva, A.P. Sirotina, E.A. Pershina, A.M. Tagachenkov, Y.V. Anufriev, E.V. Zenova, N.V. Porokhov, M.A. Tarkhov. Supercond. Sci. Technol. **34**, *8*, 085016 (2021). https://doi.org/10.1088/1361-6668/ac0d09
[7] Z. Yang, X. Wei, P. Roy, D. Zhang, P. Lu, S. Dhole, H. Wang, N. Cucciniello, N. Patibandla, Z. Chen, H. Zeng, Q. Jia, M. Zhu. Materials **16**, *23*, 7468 (2023). https://doi.org/10.3390/ma16237468
[8] S. Guo, Q. Chen, D. Pan, Y. Wu, X. Tu, G. He, H. Han, F. Li, X. Jia, Q. Zhao, H. Zhang, X. Bei, J. Xie, L. Zhang, J. Chen, L. Kang, P. Wu. Sci. Rep. **10**, *1*, 9057. (2020). https://doi.org/10.1038/s41598-020-65901-5
[9] S.N. Dorenbos. Superconducting Single Photon Detectors. Gildeprint, Enschede. Delft-Leiden (2011). (172) ISBN: 978-90-8593-017-2
[10] I. Filippov, A. Anikanov, A. Rykov, A. Mumlyakov, M. Shibalov, I. Trofimov, N. Porokhov, Y. Anufriev, M. Tarkhov. Supercond. Sci. Technol. **37**, *1*, 015018 (2024).
[11] B. Biswas, B. Saha. Phys. Rev. Materials **3**, *2*, 020301 (2019). https://doi.org/10.1103/PhysRevMaterials.3.020301
[12] J.M. Chevalier, S. Cichoň, J. Bulíř, M. Poupon, P. Hubík, L. Fekete, J. Lančok. AIP Adv. **9**, *1*, 015317 (2019). https://doi.org/10.1063/1.5056245
[13] B. Saha, A. Shakouri, T.D. Sands. Appl. Phys. Rev. **5**, *2*, 021101 (2018). https://doi.org/10.1063/1.5011972
[14] I. Miccoli, F. Edler, H. Pfnür, C. Tegenkamp. J. Phys.: Condens. Matter **27**, *22*, 223201 (2015). https://doi.org/10.1088/0953-8984/27/22/223201
[15] D. Destraz, K. Ilin, M. Siegel, A. Schilling, J. Chang. Phys. Rev. B **95**, *22*, 224501. (2017). https://doi.org/10.1103/PhysRevB.95.224501

Translated by I.Mazurov